

# Trace element composition of rutile and Zr-in-rutile thermometry in meta-ophiolitic rocks from the Kazdağ Massif, NW Turkey

Fırat Şengün<sup>1</sup> · Thomas Zack<sup>2</sup>

Received: 19 January 2015 / Accepted: 2 February 2016 / Published online: 10 February 2016  
© Springer-Verlag Wien 2016

**Abstract** In northwest Turkey, ophiolitic meta-gabbros are exposed on the Kazdağ Massif located in the southern part of the Biga Peninsula. Trace element composition of rutile and Zr-in-rutile temperatures were determined for meta-gabbros from the Kazdağ Massif. The Zr content of all rutiles range from 176 to 428 ppm and rutile grains usually have a homogeneous Zr distribution. The rutile grains from studied samples in the Kazdağ Massif are dominated by subchondritic Nb/Ta (11–19) and Zr/Hf ratios (20–33). Nb/Ta and Zr/Hf show positive correlation, which is probably produced by silicate fractionation. The Nb/Ta and Zr/Hf ratios increase with a decrease in Ta and Hf contents. The core of rutile grains are generally characterized by low Nb/Ta ratios of 17–18 whereas the rims exhibit relatively high Nb/Ta ratios of 19–23. Trace element analyses in rutile suggest that these rutile grains were grown from metamorphic fluids. The P-T conditions of meta-gabbros were estimated by both Fe–Mg exchange and Zr-in-rutile thermometers, as well as by the Grt-Hb-Plg-Q geothermobarometer. The temperature range of 639 to 662 °C calculated at 9 kbar using the Zr-in-rutile thermometer is comparable with temperature estimates of the Fe–Mg exchange thermometer, which records amphibolite-facies metamorphism of intermediate P-T conditions. The P-T conditions

of meta-ophiolitic rocks suggest that they occur as a different separate higher-pressure tectonic slice in the Kazdağ metamorphic sequence. Amphibolite-facies metamorphism resulted from northward subduction of the İzmir-Ankara branch of the Neo-Tethyan Ocean under the Sakarya Zone. Metamorphism was followed by internal imbrication of the Kazdağ metamorphic sequence resulting from southerly directed compression during the collision.

## Introduction

Rutile (TiO<sub>2</sub>) is an important accessory mineral in a variety of magmatic and metamorphic rocks, and occurs as a detrital mineral in sedimentary rocks. It is commonly found in high-grade metamorphic rocks from oceanic and continental subduction zones (e.g. Foley et al. 2002; Zack et al. 2002; Meinhold 2010; Ding et al. 2013). Rutile from these medium-grade metamorphic rocks can provide insights into petrological and chemical histories of subduction zones and also constrain metamorphic temperatures in subduction zone processes.

Rutile is a major titanium-bearing phase that carries the high field strength elements (HFSE's) and dominates the Nb, Ta and Ti budgets of many rocks in subduction zone systems (Brenan et al. 1994; Green 1995; Foley et al. 2000; Rudnick et al. 2000; Ding et al. 2013). It can also accommodate a wide range of highly charged trace elements up to the percent level, such as V, Cr, Fe, Al, Sn, Sb and W (e.g. Graham and Morris 1973; Deer et al. 1992; Zack et al. 2002). Nb/Ta ratios of rutile have been used for geochemical tracing of the crust-mantle differentiation through subduction zone metamorphism (Schmidt et al. 2008; Ding et al. 2009; Meinhold 2010).

Zr-in-rutile thermometer is based on the zirconium content in rutile coexisting with quartz and zircon. Zirconium

---

Editorial handling: D. Frei

✉ Fırat Şengün  
firsatsengun@comu.edu.tr

<sup>1</sup> Terzioğlu Campus, Faculty of Engineering, Department of Geological Engineering, Çanakkale Onsekiz Mart University, 17100 Çanakkale, Turkey

<sup>2</sup> Department of Earth Sciences, University of Gothenburg, Box 460, 40530 Gothenburg, Sweden

incorporation in the rutile crystal lattice is strongly dependant on temperature in quartz-and zircon-bearing systems, which allowed the development of Zr-in-rutile thermometers (Zack et al. 2004; Watson et al. 2006; Ferry and Watson 2007; Tomkins et al. 2007). This thermometer is a powerful single-mineral thermometer and has been commonly applied to constrain metamorphic temperatures of medium to high-grade and ultra high-grade metamorphic rocks (e.g. Spear et al. 2006; Zack and Luvizotto 2006; Zhang et al. 2009; Meyer et al. 2011; Ewing et al. 2013; Gao et al. 2014).

The metamorphic sequence of the Kazdağ Massif has been previously described as a metamorphic complex consisting of various gneisses, amphibolites, marbles and meta-ophiolites (Okay et al. 1996, 2006; Duru et al. 2004). However, internal succession, contact relations of various rock types, and origin of assembly remain under debate. The main questions regarding the metamorphic evolution and tectonic setting of the meta-ophiolites also remain unanswered.

Rutile geochemistry combined with Zr-in-rutile thermometers can allow us to evaluate the trace element behaviour of subducted oceanic crust and metamorphic evolution in subduction zone processes. In this study Fe-Mg exchange, Zr-in-rutile thermometers and Grt-Hb-Plg-Q geothermobarometer are applied to estimate metamorphic P-T conditions of meta-ophiolitic rocks. The Zr-in-rutile thermometer is examined to check how well it fits with conventional thermometers, with the aim of assessing how reliable this thermometer is for subduction systems. This study focuses on the trace element composition of rutile and application of Zr-in-rutile thermometry to meta-gabbros from the meta-ophiolitic rocks in the Kazdağ Massif located in the northwest of Turkey (Fig. 1). The purpose of this study is to provide first insights into the metamorphic evolution of subducted oceanic crust and estimate the metamorphic temperature of meta-ophiolitic rocks.

## Geological setting

Turkey is commonly subdivided into several tectonic terrains separated by ophiolitic suture zones representing the closure of branches of Tethyan ocean basins during the Mesozoic and Cenozoic (Fig. 1) (e.g. Şengör and Yılmaz 1981; Okay and Tüysüz 1999; Moix et al. 2008). These are, from north to south, the Sakarya Zone (Okay 1984), the İzmir-Ankara Zone (Şengör and Yılmaz 1981), the Tavşanlı Zone (Okay 1986), the Afyon Zone (Okay 1984), and the Menderes Massif (Dürr et al. 1978).

The Kazdağ Massif lies in the Sakarya Zone and is located in the south of the Biga Peninsula of northwest Turkey (Fig. 2), which is a region where different tectonic units, crustal fragments and oceanic assemblages of different origins and ages meet (Okay and Satır 2000; Beccalotto and Jenny 2004; Şengün et al. 2011; Aysal et al. 2012). The Kazdağ Massif

structurally forms a NE-SW – plunging anticlinorium of medium to high-grade metamorphic rocks representing the deepest section of continental crust exposed in northwest Turkey (Schuiling 1959; Bingöl 1969; Okay et al. 1991; Okay and Satır 2000; Duru et al. 2004). The Kazdağ Massif is generally regarded as a Late Oligocene metamorphic core complex (Okay et al. 1991; Okay and Satır 2000). The medium-grade metamorphic basement rocks of the Kazdağ Massif are mainly composed of felsic gneisses, amphibolite, marble and meta-ophiolitic rocks at the basal – middle part of the massif, and metagranite associated migmatite, amphibolite, and marble intercalations at the top (Fig. 3) (e.g. Okay et al. 1991; Duru et al. 2004; Erdoğan et al. 2013; Yiğitbaş et al. 2014).

The meta-ophiolitic rocks of the Kazdağ Massif occur in the core of the anticlinorium enveloped by a marble-rich sequence, which passes up to felsic gneisses with migmatite, marble and amphibolite (Bingöl 1969; Pickett et al. 1996; Okay and Satır 2000; Duru et al. 2004; Erdoğan et al. 2013). The meta-ophiolitic rocks, a typical oceanic assemblage, consist of meta-ultramafic rocks and dark-green coloured, banded meta-gabbro (Fig. 3). The meta-ultramafic rocks are dominated by massive meta-pyroxenite and meta-dunite that is partly serpentinized. The meta-gabbros are generally foliated and their primary texture is widely preserved. This unit is tectonically overlain by a marble-gneiss sequence (Duru et al. 2004; Yiğitbaş et al. 2014).

The metamorphic rocks of the Kazdağ Massif underwent amphibolite to granulite-facies metamorphism under progressive compression during the Alpine orogeny, associated with the emplacement of metagranites (Okay and Satır 2000; Erdoğan et al. 2013). Zircon ages from felsic gneisses and amphibolite in the Kazdağ Massif determined by single-zircon stepwise Pb evaporation method are  $308 \pm 16$  Ma and  $329 \pm 5$  Ma, respectively. However, K-Ar mica ages from two gneisses in the Kazdağ Massif yielded  $26 \pm 3$  Ma and  $27 \pm 3$  Ma which are related to the Alpine overprint (Bingöl 1969). Okay and Satır (2000) reported Rb/Sr muscovite and biotite ages clustering at 24–20 Ma and 20–18 Ma from gneiss samples, respectively. More recently, U-Pb zircon ages from metagranite samples yielded  $24.8 \pm 4.6$  Ma and  $28 \pm 10$  Ma, which is interpreted as migmatitic metamorphism in the Kazdağ Massif occurring during the Alpine orogeny (Erdoğan et al. 2013). This isotopic data suggests that medium-grade metamorphism in the Kazdağ Massif occurred during the Carboniferous and during the late Oligocene (Okay et al. 1996; Okay and Satır 2000; Erdoğan et al. 2013; Yiğitbaş et al. 2014). Apatite fission-track ages of 17–14 Ma from the Alakeçi shear zone located on the western flank of the Kazdağ Massif were linked to exhumation of the Kazdağ Massif (Cavazza et al. 2009). The Kazdağ Massif may be compared to the Rhodope Massif in Greece in terms of lithology and timing of metamorphism (e.g. Beccalotto and Jenny 2004; Okay et al. 1996; Okay and Satır 2000).

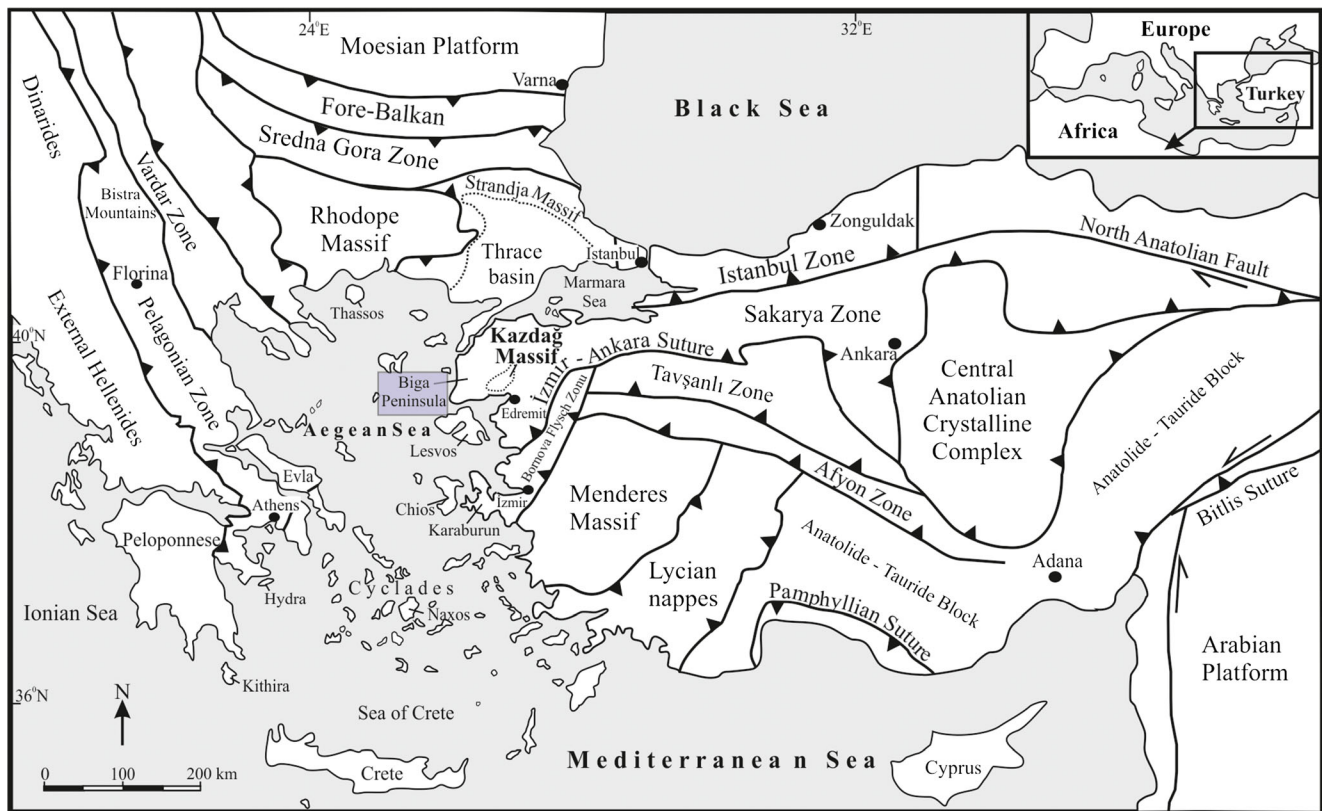


**Fig. 1** Tectonic map of the Eastern Mediterranean region indicating the major geotectonic units and the bounding sutures (modified from Okay et al. 2006; Meinhold et al. 2010)

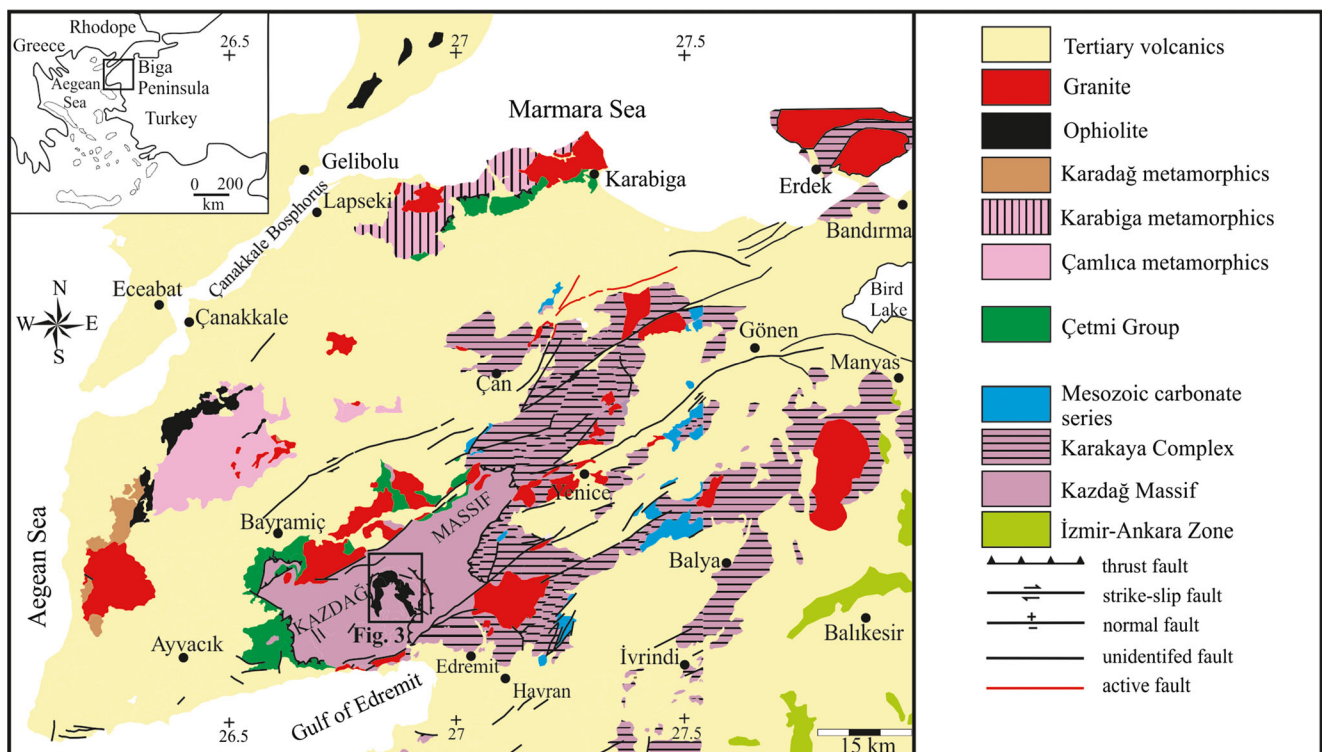


**Fig. 2** Generalized geological map of the Biga Peninsula (modified from MTA 2012). Inset map shows location of the Biga Peninsula



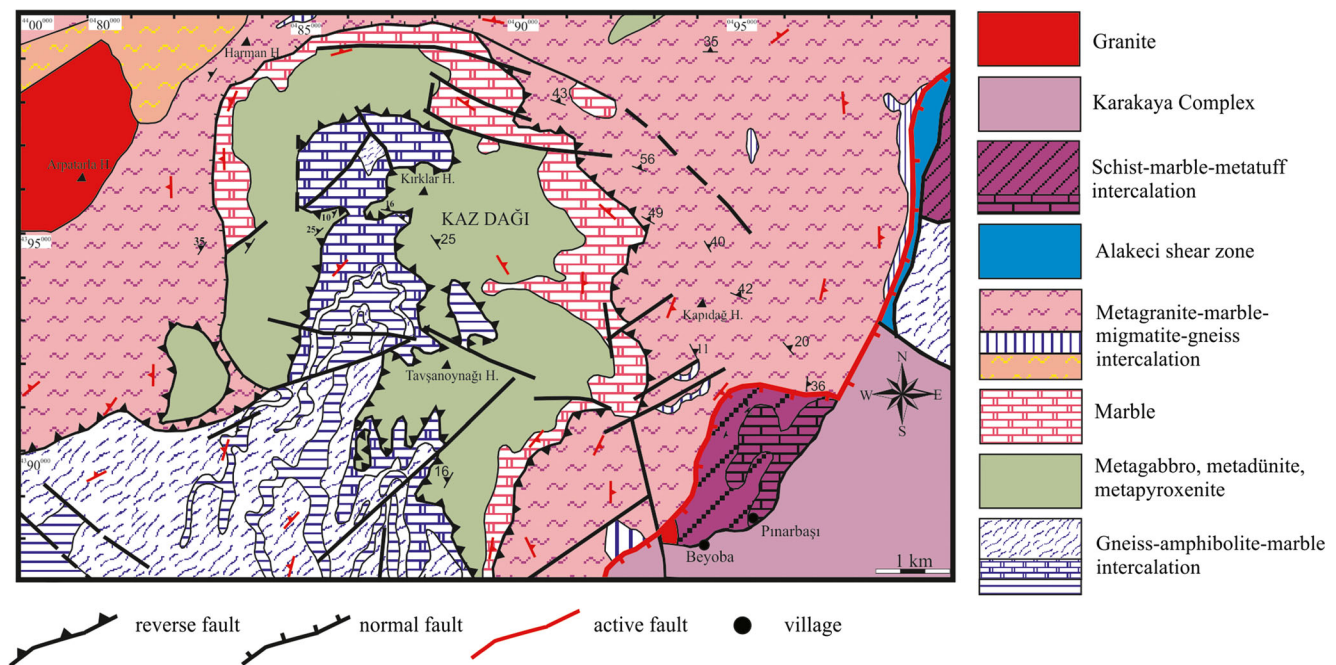


**Fig. 3** Detailed geological map of the meta-ophiolitic rocks in the Kazdağ Massif (modified from Duru et al. 2004)

The medium-grade metamorphic rocks of the Kazdağ Massif are tectonically overlain by the Permo-Triassic Karakaya Complex, comprising low-grade metamorphic and sedimentary rocks, subduction-accretionary intra-oceanic arc/forearc units marking the closure of the Palaeotethyan oceanic domain (Okay et al. 1996; Okay and Göncüoğlu 2004).

## Petrography

The studied samples were taken from meta-gabbros of the meta-ophiolitic rocks, which is the dominant rock type including rutile minerals. Meta-gabbros (1130, 1184, 1202, 1301) contain 45.3–51.7 wt% SiO<sub>2</sub>, and 15.65–16.8 wt% Al<sub>2</sub>O<sub>3</sub>. Samples are characterized by MgO contents of 7.53–10.05 wt% and TiO<sub>2</sub> concentrations ranging from 0.41 to 1.37 wt%. CaO content is fairly high (11.05–13.08 wt%). They have low K<sub>2</sub>O (0.05–0.35 wt%) and high Na<sub>2</sub>O (1.69–2.53 wt%). Their Mg# values vary from 44 to 60, and are importantly lower than the reference value for primary basaltic magma (Frey et al. 1978). All meta-gabbro samples display poikilitic and nematoblastic textures. The main mineral assemblage of meta-gabbro is dominated by plagioclase (~40 vol.%), hornblende (~30 vol.%), clinopyroxene (~15 vol.%), orthopyroxene (~5 vol.%), and biotite (~5 vol.%). Accessory mineral phases include garnet, epidote, chlorite, Ca-amphibole, quartz, rutile, titanite, zircon, apatite and ilmenite. Inclusion of quartz, epidote and zircon occur in minor porphyroblastic garnet. Rutile grains do not show the presence of inclusions (Fig. 4a) and occur either as 80 to 90 µm separate grains in matrix, or as small inclusions (<20 µm) in

clinopyroxene. They are mostly dark brown and have thin ilmenite overgrowth (Fig. 4b). Small zircons (<30 µm) are present either in garnet or matrix. Some rutile grains have a retrograde rim of titanite. Pseudomorphic replacement of garnet by chlorite-epidote-amphibole assemblage, and rutile enveloped by titanite indicate gradual retrogression into greenschist-facies rocks.

## Sample preparation and analytical methods

### Sample preparation

Samples were prepared for trace element analysis as polished thin sections of 50 µm (1184, 1202) and grain mounts (1130, 1301). Photomicrographs were taken to identify the exact spots for laser ablation analysis and prepared for orientation using reflected light in the laser ablation sample cell. However, rutile grains from meta-gabbro (1130, 1301) were firstly concentrated by crushing, sieving, heavy liquid, magnetic separation and hand picking under the binocular microscope. These rutile grains were mounted in epoxy for trace element analysis and then well polished. Transmitted-and reflected light images were taken to define their position in the mount. Backscattered electron (BSE) images were obtained using a Hitachi S-3400 N scanning electron microscope (SEM) at the University of Gothenburg to identify inclusions in rutile and document the most suitable spots for analysis. The operation conditions during the BSE imaging were maintained at 20 kV and 6.04 nA. Samples were cleaned by polishing with 1 µm alumina oxide powder to remove any

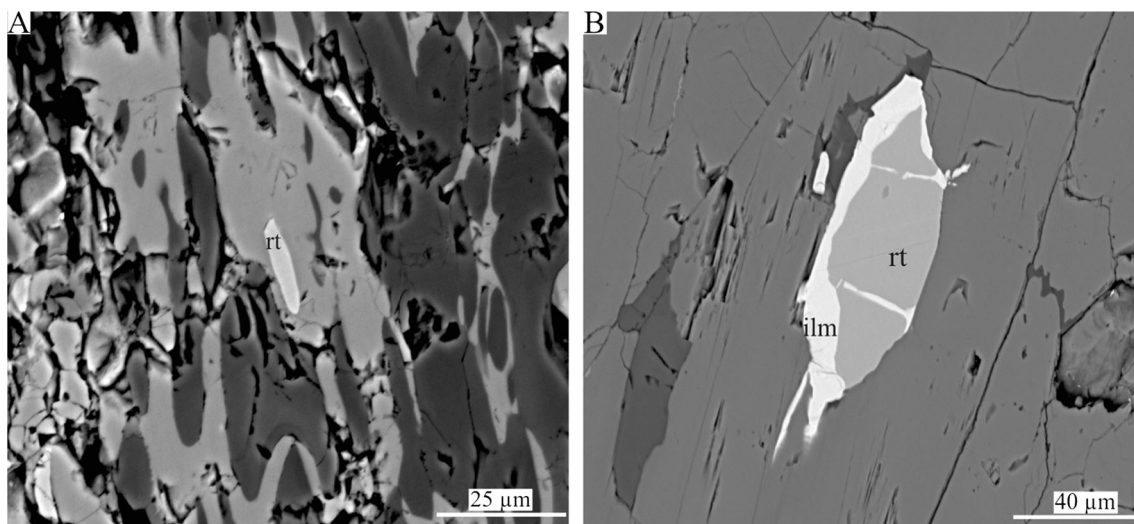


**Fig. 4** Back scattered electron (BSE) images showing the textural relationships. **a** rutile (rt) grains occurring in the matrix. **b** rutile is surrounded by ilmenite (ilm) rim

carbon coating residual from SEM analysis. Then samples were put in an ultrasonic cleaning bath for 5 min and dried with ethanol-soaked tissue wiper to remove remaining surface contamination prior to being loaded into the laser ablation sample chamber.

#### LA-ICPMS analysis

The in situ trace element analyses of rutile were performed on prepared thick sections and grain mounts at the Department of Earth Sciences at the University of Gothenburg. All samples were analysed using New Wave NWR 213 laser ablation system coupled to an Agilent 8800 QQQ quadrupole ICP-MS. A He-Ar mixture was used as carrier gas. Helium gas, which carries the laser ablated sample aerosol from the sample cell, is mixed with argon carrier gas and nitrogen as additional diatomic gas to enhance sensitivity, and finally flows into the ICPMS torch. Helium is flushed through the ablation cup at  $\sim 1$  ml/min. The helium reduces surface deposition during ablation, which increases sensitivity and also reduces fractionation owing to particle size bias (Eggins et al. 1998).

Trace elements in rutile were analysed using laser beam with diameter of 12  $\mu\text{m}$  at laser energy of  $\sim 7.7$  J/cm<sup>2</sup> and a repetition rate of 5 Hz. Signals were recorded over 60 s for each spot. The first 20 s were used to acquire background subtraction during laser warm-up. The following 30 s of dwell time were used for analysis of the sample by the ablation of rutile. The last 10 s were used for wash out. <sup>27</sup>Al, <sup>51</sup>V, <sup>53</sup>Cr, <sup>57</sup>Fe, <sup>178</sup>Hf, <sup>181</sup>Ta, <sup>232</sup>Th (10 ms dwell time), <sup>49</sup>Ti, <sup>93</sup>Nb (5 ms dwell time) and <sup>90</sup>Zr, <sup>238</sup>U (30 ms dwell time) were analysed for trace element concentration in rutile. Each standard block is composed of two analyses of the R10 rutile standard and two analyses of NIST SRM 610 glass standard. Titanium measured as <sup>49</sup>Ti was used as internal standard element for all analyses. <sup>90</sup>Zr was used to

determine the Zr concentration of rutile. The glass reference material NIST SRM 610 (Jochum and Nehring 2006) and R10 (Luvizotto et al. 2009) rutile were used for external calibrations. The concentrations of elements were determined using “GLITTER version 4.4.4” software; (On-line interactive data reduction for LA-ICPMS microprobe (van Achterbergh et al. 2000) on the basis of measurements of the following isotopes: <sup>49</sup>Ti, <sup>51</sup>V, <sup>53</sup>Cr, <sup>57</sup>Fe, <sup>90</sup>Zr, <sup>93</sup>Nb, <sup>95</sup>Mo, <sup>118</sup>Sn, <sup>121</sup>Sb, <sup>178</sup>Hf, <sup>181</sup>Ta, <sup>182</sup>W, <sup>208</sup>Pb, <sup>232</sup>Th, and <sup>238</sup>U. Titanium content during data reduction was initially assumed to be 100 wt% TiO<sub>2</sub>. The mean detection limits (99 % confidence level) of the elements determined for all minerals were <sup>90</sup>Zr = 0.017 ppm, <sup>93</sup>Nb = 0.011 ppm, <sup>178</sup>Hf = 0.021 ppm, <sup>181</sup>Ta = 0.004 ppm.

For temperature calculations, the following calibrations of the Zr-in-rutile thermometer were applied: Zack et al. (2004), Watson et al. (2006), Ferry and Watson (2007), and Tomkins et al. (2007).

## Results

### Trace element composition of rutile

Representative trace element concentrations of rutile grains are given in Table 1. Rutile occurs as three different textural types in the studied samples. The most frequent type in samples (1184, 1202) is matrix rutile with a grain size between 80 and 90  $\mu\text{m}$ . Rutile occurs as an inclusion in garnet (grain size of rutile: 20–40  $\mu\text{m}$ ) and in clinopyroxene (grain size of rutile: 10–20  $\mu\text{m}$ ). Moreover, larger crystals separated from meta-gabbros (1130, 1301) with a grain size between 100 and 300  $\mu\text{m}$  form intergrowths with ilmenite. The different textural rutile types in meta-gabbros and the associated range of Zr concentrations are summarized in Table 2. Most

**Table 1** LA-ICPMS trace element concentrations and estimated temperatures of rutile by Zr-in-rutile thermometry

Elements (ppm)	Grain no	V	Cr	Fe	W	Zr	Nb	Hf	Ta	Nb/Ta	Zr/Hf	T1	T2	T3	T4
Sample no															
1130	3	903	3162	1869	21	267	186	8	8	23	32	704	633	634	637
	3	903	2988	1655	19	268	180	9	9	20	30	704	633	634	637
	3	914	2854	1642	18	248	182	8	11	17	30	695	627	628	632
	3	927	2770	1885	29	254	191	8	11	17	31	698	629	630	633
	2	1013	2914	2013	41	305	218	10	11	19	30	721	644	645	647
	1	971	3282	1954	24	313	216	10	12	18	32	725	646	647	650
	5	1129	2349	2525	69	314	326	10	26	13	33	725	646	647	650
	4	843	2287	1433	21	287	212	14	11	19	20	713	639	640	643
	4	848	2282	2631	26	259	209	12	11	18	23	700	631	632	635
	4	876	2383	1710	24	299	224	12	12	19	26	718	642	643	646
	14	938	3472	2030	29	292	216	11	12	18	27	715	640	641	644
	14	940	3525	2729	27	302	202	10	11	18	30	720	643	644	647
	11	949	2688	2959	32	266	228	9	12	19	29	704	633	634	637
	10	957	2710	2294	25	286	234	10	14	16	27	713	639	640	642
	9	1238	2188	1662	51	176	363	8	28	13	23	651	601	602	606
	8	876	1777	1253	56	237	228	9	18	13	26	689	624	625	628
	13	919	2745	1376	17	285	120	9	8	15	32	712	638	639	642
	12	1069	1674	2182	20	274	223	8	18	12	33	707	635	636	639
	15	1027	3620	2017	36	352	200	12	14	14	30	739	656	656	659
<b>Avg</b>												<b>708</b>	<b>636</b>	<b>637</b>	<b>640</b>
1184	21	1140	1167	2911	22	323	811	11	45	18	29	728	648	649	652
	22	793	2169	1485	212	289	765	12	49	16	24	714	639	640	643
	23	1126	1171	2525	10	428	748	18	40	19	24	764	672	673	675
	25	1297	1226	1041	33	357	796	10	41	19	36	741	657	658	660
	26	704	1892	1516	41	378	802	16	46	17	24	748	662	662	664
	27	817	1658	1467	30	391	759	10	40	19	39	753	665	665	667
	30	813	2140	1476	32	420	754	14	39	19	30	762	671	671	673
	<b>Avg</b>												<b>745</b>	<b>659</b>	<b>660</b>
1202	45	1104	3437	6816	85	302	779	11	73	11	27	720	643	644	647
	46	710	3355	2464	93	250	721	9	62	12	27	695	628	629	632
	47	926	2878	2620	66	278	748	10	64	12	28	709	636	637	640
	48	758	3216	2854	69	274	760	11	69	11	25	707	635	636	639
	<b>Avg</b>												<b>708</b>	<b>635</b>	<b>636</b>
1301	50	1213	1380	1784	25	381	176	13	8	22	30	750	662	663	665
	51	939	1444	2065	57	176	258	9	17	15	20	650	601	602	606
	52	959	2396	2883	31	333	336	14	18	19	23	732	651	652	654
	53	1191	1590	2099	103	301	248	10	18	14	30	719	643	644	646
	54	889	2932	2533	15	209	125	8	7	18	26	673	614	615	619
	55	836	1131	2820	19	340	226	15	18	13	23	735	653	654	656
	56	1119	1917	2158	44	236	210	10	10	21	24	689	623	625	628
	57	943	2368	2049	35	399	306	13	16	19	31	755	666	667	669
<b>Avg</b>												<b>717</b>	<b>641</b>	<b>642</b>	<b>643</b>

1, 2, 3, 4 Temperatures were estimated according to the thermometry of Zack et al. (2004), Watson et al. (2006), Ferry and Watson (2007), and Tomkins et al. (2007) at 9 kbar, respectively

Average temperatures are given in bold

**Table 2** Zr concentrations in different positions of rutile grains

Sample	1184 Zr (ppm)	1202 Zr (ppm)
Rt in matrix	357	250
	378	274
	391	
Rt in garnet	420	302
	428	278
Rt in clinopyroxene	289	
	323	

porphyroblastic garnet grains exhibit small cracks containing retrograde minerals such as chlorite, epidote and biotite, indicating possible pathways for trace element transfer during retrogression. Rutile from sample 1130 has Zr and Hf concentrations of 176–352 ppm and 8–14 ppm. The Nb and Ta contents vary from 180 to 363 ppm and from 8 to 28 ppm. The Zr and Hf concentrations of rutile from sample 1184 range between 289 and 428 ppm and 10 and 18 ppm, respectively, whereas their Nb and Ta concentrations vary between 748 and 811 ppm and 39 and 49 ppm. Rutile from sample 1202 has Zr and Hf contents of 250–302 ppm and 9–11 ppm, respectively. The Nb and Ta concentrations vary from 721 to 779 ppm and from 62 to 73 ppm. Rutile from sample 1301 has Zr and Hf contents of 176–399 ppm and 8–15 ppm, respectively. The Nb and Ta concentrations in rutile in this sample range from 125 to 336 ppm and from 7 to 37 ppm. V and Cr contents of rutile grains from meta-gabbro samples range from 704 to 1238 ppm and 1131 to 3620 ppm, respectively. However, a rutile grain from sample 1202 shows the highest Fe concentration of 6816 ppm.

BSE images of several rutile grains suggest the absence of systematic compositional zoning. Rutile grains were analysed with multiple spots which usually have a homogeneous Zr distribution (Fig. 5). However, in some places the rim is slightly enriched in Zr (Fig. 5a, b). The Zr-rich phase separations are responsible for the variation of Zr concentrations in this rutile grain. A replacement by rutile of a pre-existing Zr-rich mineral like ilmenite is a possible explanation for the formation of these Zr-rich phase separations in rutile (Austrheim et al. 2008; Meyer et al. 2011).

The propagation in concentrations and element ratios changes from sample to sample, which is more pronounced for Nb and Ta elements than Zr and Hf elements. Nb and Ta exhibit a strong positive correlation (Fig. 6a). Zr and Hf also indicate a positive correlation, but less distinct (Fig. 6b). On the other hand, Ta and Zr show a poor correlation (1184), although three samples (1202, 1130, 1301) indicated a positive correlation (Fig. 6c).

Both Nb/Ta and Zr/Hf show an increased variation with a decrease in Ta and Hf concentrations (Fig. 7a, b). Rutile compositions mostly display subchondritic Nb/Ta values

(chondritic value 19.9, Münker et al. 2003) with a range of 11–19 and Zr/Hf values (chondritic value  $34.3 \pm 0.3$ , Münker et al. 2003) range between 20 and 33 (Fig. 7c). However, two rutile grains from sample 1301 and sample 1130 have suprachondritic Nb/Ta and Zr/Hf values.

### Zr-in-rutile thermometry and conventional geothermobarometry

The average Zr concentrations and corresponding Zr-in-rutile temperatures are given in Table 1. The Zr contents of rutile grains range between 176 and 428 ppm. Temperatures of rutile were calculated according to the Zr-in-rutile thermometry by Zack et al. (2004), Watson et al. (2006) Ferry and Watson (2007), Tomkins et al. (2007), and Fe-Mg exchange thermometers. The calibration of Zack et al. (2004) yielded temperatures of 708–745 °C with an average temperature of 720 °C. These temperature estimations are higher than the temperatures estimated using other calibrations. Temperatures calculated by using the calibration of Watson et al. (2006) range between 635 and 659 °C. This estimation has an average temperature of 643 °C. The calibration of Ferry and Watson (2007) yielded temperatures of 636–660 °C with an average temperature of 644 °C. The temperatures of Watson et al. (2006) and Ferry and Watson (2007) are rather similar to each other. The Zr-in-rutile thermometer by Tomkins et al. (2007) is pressure dependent. However, pressure estimations for rutile from meta-gabbro in the study area were unknown. Representative mineral compositions of garnet, hornblende, biotite and plagioclase are summarized in Table 3. The Blundy and Holland (1990) amphibole-plagioclase geothermometer yielded a temperature of ~660 °C. The garnet-biotite Fe-Mg exchange thermometer of Ferry and Spear (1978) gives temperatures of 640 to 690 °C for meta-gabbros. The widely used garnet-hornblende-plagioclase-quartz geobarometer (Kohn and Spear 1990) yielded pressure of 9 kbar at a temperature of 660 °C for the four meta-gabbros. Based on conventional geothermobarometers, a reasonable estimate for the peak P-T conditions in the meta-ophiolitic rocks is 9 kbar and  $665 \pm 25$  °C. At 9 kbar, the Zr-in-rutile thermometer of Tomkins et al. (2007) gives 639–662 °C with an average temperature of 646 °C. This estimated temperature is consistent with the stability fields of rutile determined by Perple\_X for MORB (mid-ocean ridge basalt) composition (John et al. 2011).

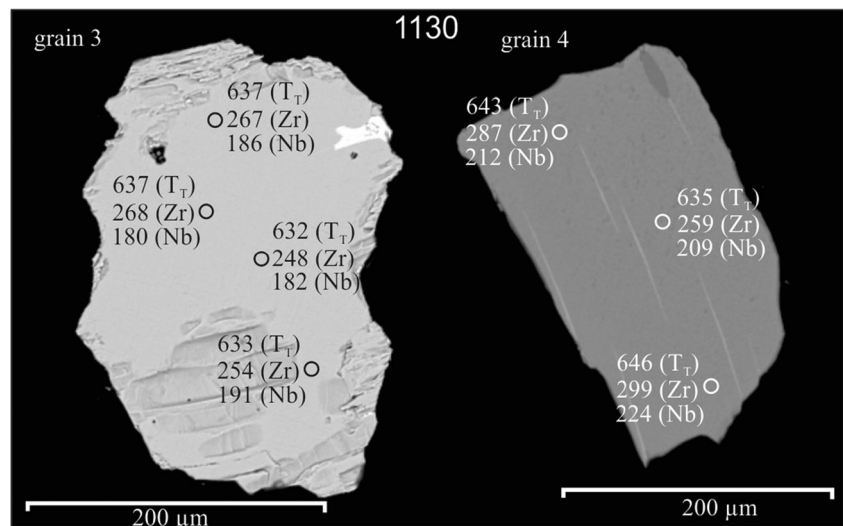
## Discussion

### Trace element characteristics of rutile

Nb and Ta in rutile would dominate the whole rock Nb and Ta budget, and the average Nb/Ta ratio of rutile may be identical to that of the bulk rock. Rutile grains from all meta-gabbros



**Fig. 5** BSE images of rutile from sample 1130 (grain 3 and grain 4) used for multiple measurements. **a–b** Rutile grain with homogeneous Zr content throughout the grain but the rim is slightly enriched in Zr content. Ilmenite needles occur in rutile. Circles mark the location of the spots analysed. The numbers give  $T_T$  in  $^{\circ}\text{C}$  and the contents of Zr and Nb in ppm. Calculated temperatures vary from 632 to 646  $^{\circ}\text{C}$  indicating a homogenous distribution of Zr-in-rutile



have not only high HFSE contents such as Nb (180–811 ppm), Ta (8–73 ppm), Zr (176–428 ppm), Hf (8–18 ppm), and W (10–103 ppm), but also high concentrations of transition metal elements such as V (704–1238 ppm) and Cr (1131–3620 ppm). Other trace elements have low concentrations or are below the detection limits. However, it is possible that the highest Fe content (6816 ppm) from one rutile grain (sample

1202) results from analysis of microscale mineral inclusions in the form of tiny ilmenite or iron oxide lamellae. Rutile minerals from two meta-gabbro samples (1184, 1202) have high Nb and Ta concentrations, whereas rutile grains from two samples (1130, 1301) include lower Nb and Ta concentrations (Table 1, Fig. 6a). It is likely that minerals with higher Ti contents have more influence on the behaviour of Nb and

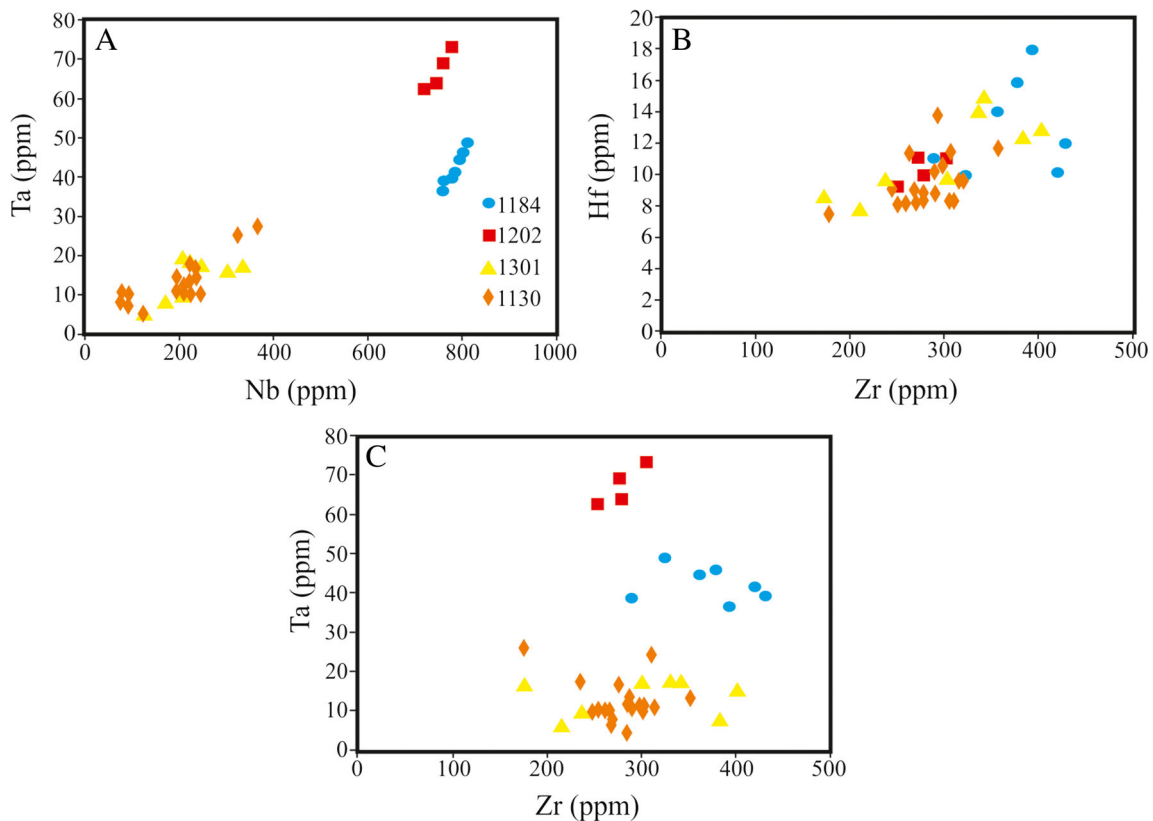


**Fig. 6** Results for HFSE concentrations of rutile from metagabbros in the Kazdağ Massif. Points refer to individual analyses. **a** Nb versus Ta indicating a strong positive correlation. **b** Zr versus Hf also show

positive correlation, but less distinctly. **c** Zr versus Ta showing negative correlation except one sample (1202)



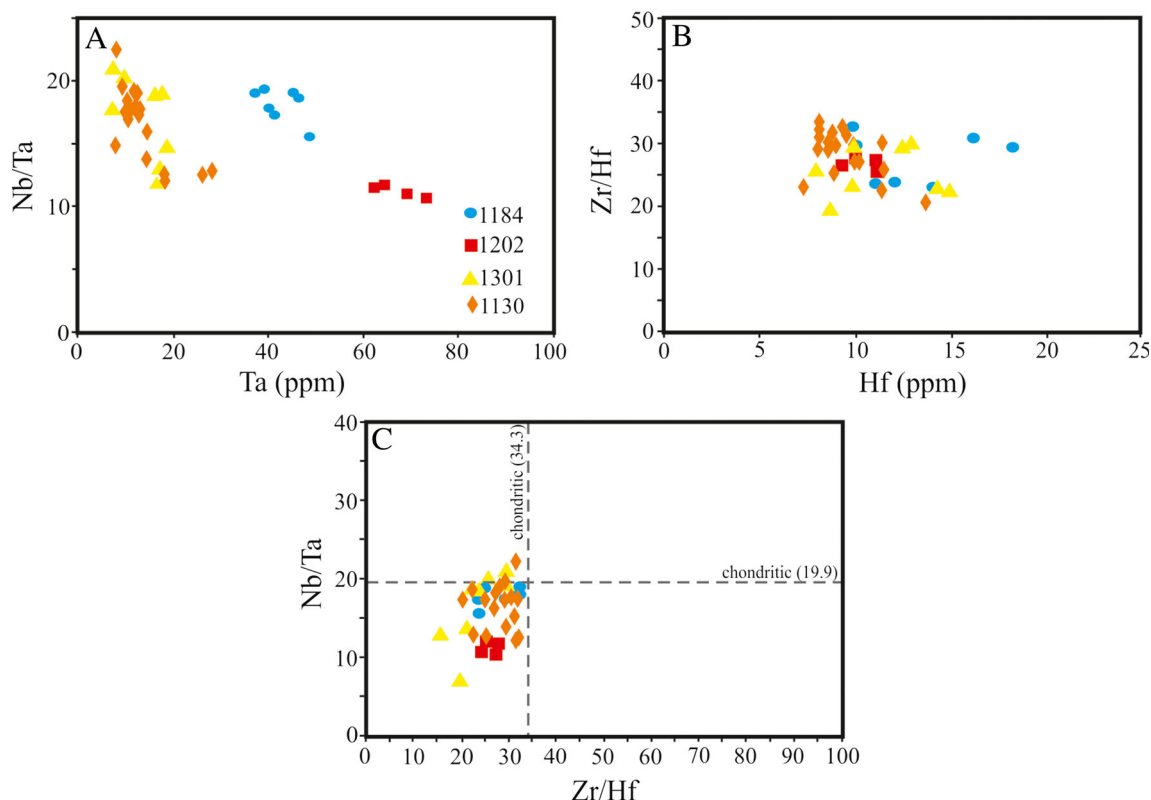


**Fig. 7** Element ratio plots. Points represent individual analyses. **a** Ta versus Nb/Ta. **b** Hf versus Zr/Hf. **c** Zr/Hf versus Nb/Ta diagram. Generally Nb/Ta and Zr/Hf of rutile are subchondritic. Dashed lines refer to chondritic values for Nb/Ta and Zr/Hf (Münker et al. 2003)

Ta owing to similar ionic radii and valence of Nb, Ta and Ti (Hornig and Hess 2000; Schmidt et al. 2004).

Nb/Ta ratios for rutile rims and cores are different from one another in one sample. The cores of rutile grains from sample 1130 are generally characterized by low Nb/Ta ratios of 17–18 whereas the rims exhibit relatively high Nb/Ta ratios of 19–23. The enrichment of Nb and Ta with slightly high Nb/Ta ratios in the rims of rutile may result from breakdown of hydrous minerals such as biotite (Stepanov and Hermann 2013), which is equivalent to crystallization from a kind of geofluid that has a high content of water-insoluble trace elements (Zheng et al. 2011; Gao et al. 2014). Based on experimental data, the partition coefficients of Nb and Ta in rutile, usually displayed for any given rutile/melt pair,  $D_{\text{Nb}}$  is always lower than  $D_{\text{Ta}}$  during the subduction processes (Schmidt et al. 2004; Klemme et al. 2005). Experimental studies also show that partitioning of Nb and Ta between rutile and fluid/melt generally gives  $D_{\text{Nb/Ta}} > 1$  (e.g. Brenan et al. 1994; Stalder et al. 1998; Xiong et al. 2005; Xiao et al. 2006). Moreover, rutile preferentially incorporates Ta over Nb during dehydration melting (Schmidt et al. 2004). If rutile was in equilibrium with such a melt, this could give rise to low Nb/Ta ratios in the initially grown rutile (Schmidt et al. 2009). Thus, the distinction of the behaviour of Nb/Ta fractionation specifies the compatibilities of Nb and Ta in rutile during rutile growth, which may be the basic result of Nb/Ta fractionation during metamorphic

dehydration in subduction zones (Gao et al. 2014). Fluid activity may drive the variations in the partitioning of Nb and Ta between fluid and rutile.

Nb/Ta and Zr/Hf show positive correlation, which is probably produced by silicate fractionation (Münker et al. 2003; Weyer et al. 2003; Schmidt et al. 2009). The continental crust, volcanic rocks, oceanic basalts and island arcs are characterized by subchondritic Nb/Ta ratios (e.g. Green 1995; Rudnick et al. 2000; Foley et al. 2002; Schmidt et al. 2009). Subchondritic Nb/Ta ratios occur in rutile from both medium to high-grade metamorphic regions (e.g. Meyer et al. 2011; Luvizotto and Zack 2009; Ewing et al. 2013) and HP metamorphic regions (Xiao et al. 2006; John et al. 2011; Huang et al. 2012). Nb/Ta and Zr/Hf ratios increase with a decrease in Ta and Hf contents (Fig. 7a, b). Accordingly, the increase in Nb/Ta ratios with the decreased Ta content can be linked to the effect of metamorphic dehydration at subduction zones on rutile Nb/Ta differentiation (Schmidt et al. 2009; Gao et al. 2014). Dehydration metamorphism is a common mechanism for rutile formation in subduction processes. Nb and Ta have the same oxidation state and similar ionic radii (Meinhold 2010) and thus would remain tightly coupled during geochemical processes in the crust-mantle differentiation system. However, there is a significant difference in their mass, which may be a potential cause for Nb/Ta differentiation during geochemical processes.

**Table 3** Representative mineral compositions from meta-gabbros

Sample	1130		1184		1202		1221		Biotite	Garnet	
	Hornblende	Plagioclase	Hornblende	Plagioclase	Hornblende	Plagioclase	Hornblende	Plagioclase		Core	Rim
SiO <sub>2</sub>	43.26	59.20	51.01	51.98	45.04	57.34	46.84	63.89	47.25	37.72	37.20
TiO <sub>2</sub>	0.52	0.02	0.24	0.03	0.49	0.02	0.54	0.02	0.22	0.16	0.10
Al <sub>2</sub> O <sub>3</sub>	10.19	24.89	6.00	29.30	11.35	26.07	8.63	22.47	4.66	21.46	21.61
FeO	15.91	0.12	10.14	0.06	12.60	0.09	19.22	0.06	18.98	20.65	28.00
MnO	0.27	0.00	0.24	0.00	0.26	0.00	0.23	0.00	0.18	11.15	4.37
MgO	12.45	0.02	14.74	0.01	10.52	0.00	8.24	0.00	10.53	0.52	0.78
CaO	11.26	7.25	13.00	13.50	12.46	8.53	10.72	3.87	10.52	8.35	8.32
Na <sub>2</sub> O	1.28	7.97	0.69	4.47	1.47	7.96	1.80	9.43	1.58	0.04	0.04
K <sub>2</sub> O	2.52	0.21	2.08	0.02	3.23	0.09	2.32	0.18	0.21	0.02	0.00
Toplam	97.67	99.68	98.14	99.37	97.42	100.11	98.54	99.93	94.12	100.07	100.43
Mineral formula on the basis of											
	23 O	8 O	23 O	8 O	23 O	8 O	23 O	8 O	11 O	12 O	12 O
Si	6.559	2.639	7.639	2.368	6.829	2.562	7.213	2.824	3.438	2.996	2.493
Ti	0.059		0.028		0.056		0.063		0.024	0.019	0.012
Al(IV)	1.592	1.308	0.542	1.573	1.129	1.350	0.917	1.171		0.004	0.007
Al(VI)	0.188		0.492		0.912		0.621		0.417	1.019	2.042
Fe <sup>2+</sup>	1.102		1.240		1.607		2.430		1.163		
Fe <sup>3+</sup>	0.869		0.000		0.000		0.030			1.745	1.722
Mn	0.034		0.029		0.034		1.858		0.023	1.136	0.788
Mg	2.749		3.212		2.391		1.737		1.037	0.137	0.184
Ca	1.787	0.346	2.000	0.659	2.036	0.401	0.263	0.183	0.876	0.954	0.785
Na B	0.213	0.688	0.000	0.395	0.000	0.678	0.264	0.808	0.258		
Na A	0.156		0.197		0.436		0.448				
K	0.476	0.012	0.388	0.001	0.628	0.005		0.010	0.140		
Total	15.784	4.993	15.766	4.996	16.057	4.996	15.843	4.997	7.376	8.010	8.033
	an	66.9	an	39.4	an	63	an	81.7	alm	46.32	62.97
	ab	32.5	ab	60.5	ab	36.5	ab	17.3	pyr	2.07	3.11
	or	0.6	or	0.1	or	0.5	or	0.1	gross	24.01	23.97
									spess	27.61	9.95

Trace element analyses in rutile suggest that these rutile grains were grown from metamorphic fluids. Three types of geofluids occur in subduction zones, i.e., hydrous melt, aqueous solution and supercritical fluid, which have distinct capacities in dissolving and transporting trace elements (Hermann et al. 2006; Zheng et al. 2011). Generally, water-insoluble incompatible trace elements such as LREE and MREE can be dissolved and transported together with LILE by the hydrous melt; water-soluble incompatible trace elements such as LILE are mobile in the aqueous solution; and eventually all usually fluid-immobile incompatible trace elements such as HREE and HFSE can be dissolved and transported by the supercritical fluid under subduction-zone amphibolite to high-pressure metamorphic conditions (e.g. Tatsumi and Nakamura 1986; Scambelluri et al. 2001; John et al. 2004;

Hermann et al. 2006; Xia et al. 2010; Zheng et al. 2011; Gao et al. 2014). Moreover, it is possible for rutile to grow from distinct compositions of metamorphic fluid during subduction and exhumation of oceanic crust. This is because the breakdown of hydrous minerals is a dominant source of aqueous solutions in medium to high grade metamorphic rocks (Gao et al. 2014).

### Zr-in-rutile temperatures

Although meta-ophiolitic rocks of the Kazdağ Massif are stated to have experienced amphibolite-facies metamorphism (e.g. Okay et al. 1996; Okay and Satır 2000, Duru et al. 2004), the P-T conditions of meta-ophiolitic rocks are unknown. However, the P-T conditions of surrounding felsic

gneisses were calculated by conventional thermometers and the Thermocalc program of Holland and Powell (1990) (Okay and Satir 2000). The garnet Fe-Mg exchange thermometer of Hodges and Spear (1982) gave temperatures of 560–615 °C for sillimanite gneiss and ~650 °C for calc-silicate gneisses. The geothermometer of Ellis and Green (1979) yielded a temperature of ~650 °C for diopside-garnet pairs in the calc-silicate gneiss (Okay and Satir 2000). Pressure was estimated by the Thermocalc program and the mineral chemical data from sillimanite gneisses, which varied from  $4.5 \pm 1$  to  $5.7 \pm 1$  kbar at a temperature of 640 °C (Okay and Satir 2000). A reasonable estimate for the peak P-T conditions of medium to high-grade metamorphic rocks in the Kazdağ Massif is  $5 \pm 1$  kbar and  $640 \pm 50$  °C (Okay and Satir 2000).

The P-T conditions of meta-gabbros from four samples have been estimated at 9 kbar and  $665 \pm 25$  by using conventional geothermobarometry. However, Zr-in-rutile thermometry gave precise temperature estimates for meta-ophiolitic rocks in the Kazdağ Massif when compared to conventional thermometers. Four calibrations of the Zr-in-rutile thermometers were applied for temperature calculations. These are: Zack et al. (2004), Watson et al. (2006), Ferry and Watson (2007), and Tomkins et al. (2007). All applied calibrations gave a similar temperature range except for the calibration of Zack et al. (2004, Fig. 8), which is based on empirical and natural samples with the assemblage rutile-zircon-quartz. The Zr-in-rutile thermometer of Zack et al. (2004) gives the temperature range of 708–745 °C. These temperatures are higher than those calculated with the other calibrations (e.g. Miller et al. 2007; Baldwin and Brown 2008; Meyer et al. 2011). The temperatures calculated by this calibration in this study confirm this observation and suggest that the recent experimental calibrations are more accurate than the empirical one. Subsequently, Watson et al. (2006), Ferry and Watson (2007) and Tomkins et al. (2007) improve the thermometer resulting in more precise estimations over a wider temperature

and pressure range. The Watson et al. (2006) calibration is mainly based on experimental and natural results. The temperatures of the Watson et al. (2006) calibration range between 635 and 659 °C. Ferry and Watson (2007) defined a silica activity factor in their experimental work; i.e. the Zr concentration in rutile is not only temperature-dependant, but also sensitive to the activity of SiO<sub>2</sub>. The calibration of Ferry and Watson (2007) yielded temperatures of 636–660 °C. The experiments by Watson et al. (2006) and Ferry and Watson (2007) were conducted at identical pressure of 10 kbar, which explains the mutually compatible results for these two calibrations. Nine kbar calculated by conventional methods was used for the meta-ophiolitic rocks, which experienced a lower pressure than ~10 kbar in these experimental calibrations. Therefore, the calibration of Tomkins et al. (2007) with a pressure correction is the best choice for temperature calculation. Furthermore, the calibration of Tomkins et al. (2007) is a trustworthy thermometry for medium to high-grade metamorphic rocks, which gives more reliable temperatures than any other exchange thermometers (e.g. Spear et al. 2006; Miller et al. 2007; Luvizotto and Zack 2009). Accordingly, the significance of a pressure correction should not be ignored for rocks which not only experienced more pressure but also underwent lower pressure dominated metamorphism. It is noted that pressure used for meta-gabbro was assumed to be 9 kbar in the equation of Tomkins et al. (2007) based on a conventional geothermobarometer estimation of 9 kbar for the condition of amphibolite-facies metamorphism. The Zr-in-rutile thermometer of Tomkins et al. (2007) gives temperatures of 639–662 °C with an average temperature of 646 °C for meta-gabbro. The corresponding Zr-in-rutile temperature (average 646 °C) is in agreement with temperature estimations by conventional thermometers based on the mineral assemblage of gneisses in the Kazdağ Massif (Okay and Satir 2000). This calculated temperature range could yield temperatures of metamorphism for meta-ophiolitic rocks in the Kazdağ Massif. On the other hand, the pressure of meta-gabbros calculated by a conventional geobarometer is higher than the pressure of gneisses surrounding the meta-ophiolitic rocks. It suggests that the meta-ophiolitic rocks form as a separate tectonic slice in the Kazdağ Massif and underwent amphibolite-facies metamorphism at ~35 km according to pressure estimation, whereas the metamorphic rocks of the Kazdağ Massif underwent amphibolite-facies metamorphism at ~20 km. Metamorphism resulted from northward subduction of the İzmir-Ankara branch of the Neo-Tethyan Ocean under the Sakarya Zone. Following metamorphism, the medium to high-grade metamorphic rocks of the Kazdağ Massif were internally imbricated by southerly compression during collision. When evaluated from a tectonic point of view, the Kazdağ metamorphic sequence was imbricated along thrust faults of southward vergence after Alpine metamorphism (Erdoğan et al. 2013) and meta-ophiolitic rocks were

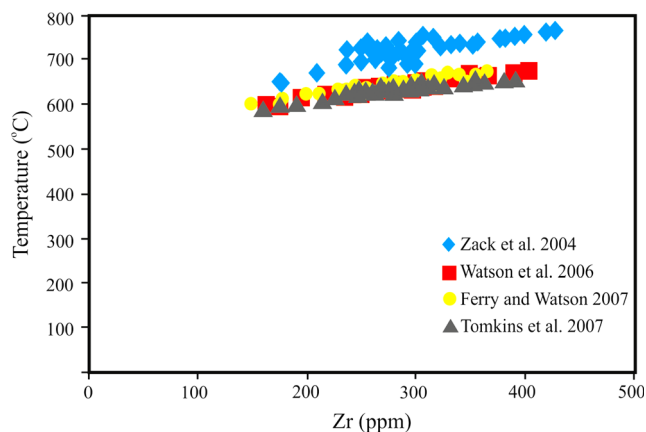


**Fig. 8** Difference in calculated temperature range of the Zr-in-rutile thermometer using various calibrations

emplaced as a different tectonic slice. Collision of the Sakarya Zone with the Anatolide-Tauride Block and internal imbrications of the Kazdağ Massif gave rise to progressive thickening in the crust.

## Conclusions

In northwest Turkey, meta-ophiolitic rocks are exposed in the Kazdağ Massif located in the southern part of the Biga Peninsula. The rutile grains from meta-gabbros in the Kazdağ Massif are dominated by subchondritic Nb/Ta and Zr/Hf ratios. The Nb/Ta and Zr/Hf ratios increase with a decrease in Ta and Hf contents, which could be ascribed to the effect of metamorphic dehydration on rutile Nb/Ta differentiation. Trace element analyses in rutile suggest that these rutile grains were grown from metamorphic fluids. An aqueous solution with high Nb/Ta ratios can be derived from metamorphic dehydration due to the breakdown of biotite during the exhumation of subducted oceanic crust. Nb and Ta are rich in rutile rims which results in slightly high Nb/Ta ratios. The enrichment of Nb and Ta in rutile rims suggests local enrichment of these water-insoluble incompatible trace elements in metamorphic fluid, which may be the product of phase separation from a supercritical fluid during exhumation.

The Zr-in-rutile thermometers and conventional geothermobarometers were applied to estimate metamorphic temperature and pressure of meta-ophiolitic rocks in the Kazdağ Massif. The peak P-T conditions of meta-ophiolitic rocks were estimated at 9 kbar and  $665 \pm 25$  based on conventional geothermobarometers. However, four calibrations of the Zr-in-rutile thermometer were applied for temperature calculations. The calibration of Tomkins et al. (2007) with a pressure correction is the best choice for temperature calculation. The Zr-in-rutile thermometer of Tomkins et al. (2007) yields temperatures of 639–662 °C (average 646 °C) at 9 kbar for meta-ophiolitic rocks in the Kazdağ Massif, which reflects the metamorphic temperature. The calibration of Tomkins et al. (2007) yielded temperature estimates for meta-ophiolitic rocks consistent with conventional thermometers. The P-T conditions of meta-ophiolitic rocks suggest that the meta-ophiolitic rocks occur as a different tectonic slice in the Kazdağ metamorphic sequence and underwent amphibolite-facies metamorphism at ~35 km. Metamorphism took place due to the northward subduction of the İzmir-Ankara branch of the Neo-Tethyan Ocean under the Sakarya Zone. The northward subduction of the İzmir-Ankara branch of the Neo-Tethyan Ocean under the Sakarya Zone was accompanied by N-S contraction during which the regionally metamorphosed Kazdağ Massif was internally imbricated. This imbrication is possibly the main reason for thickening and exhumation of the Kazdağ Massif.

**Acknowledgments** This study was supported by National Postdoctoral Research Scholarship Programme and the Scientific and Technological Research Council of Turkey (TÜBİTAK) grant 114Y834. We thank David Cornell for helping with SEM analyses. We would like to thank two anonymous reviewers and Johann Raith for valuable suggestions and editorial handling of manuscript.

## References

- Austrheim H, Putnis CV, Engvik AK, Putnis A (2008) Zircon coronas around Fe-Ti oxides: a physical reference frame for metamorphic and metasomatic reactions. *Contrib Mineral Petrol* 156:517–527
- Aysal N, Ustaömer T, Öngen S, Keskin M, Köksal S, Peytcheva I, Fanning M (2012) Origin of the Early-Middle Devonian Magmatism in the Sakarya Zone, Nw Turkey: Geochronology, Geochemistry and Isotope Systematics. *J Asian Earth Sci* 45:201–222
- Baldwin JA, Brown M (2008) Age and duration of ultrahigh-temperature metamorphism in the Anápolis Itauçu complex, Southern Brasília Belt, Central Brazil – constraints from U-Pb geochronology, mineral rare earth element chemistry and trace element thermometry. *J Metamorph Geol* 26:213–233
- Beccalotto L, Jenny C (2004) Geology and correlation of the ezine zone: A Rhodope Fragment in NW Turkey? *Turk J Earth Sci* 13:145–176
- Bingöl E (1969) Kazdağ Masifi'nin Merkezi ve GD Kesiminin Jeolojisi. *MTA Dergisi* 72:110–123
- Blundy JD, Holland TJB (1990) Calcic amphibole equilibria and a new amphibole-plagioclase geothermometer. *Contrib Mineral Petrol* 104:208–224
- Brenan JM, Shaw HF, Phinney DL, Ryerson FJ (1994) Rutile-aqueous fluid partitioning of Nb, Ta, Hf, Zr, U and Th: implications for high field strength element depletions in island-arc basalts. *Earth Planet Sci Lett* 128:327–339
- Cavazza W, Okay AI, Zattin M (2009) Rapid early-middle exhumation of the Kazdağ Massif (Western Anatolia). *Int J Earth Sci* 98:1935–1947
- Deer WA, Howie RA, Zussman J (1992) An introduction to Rock-forming minerals. Longman Group, Harlow, UK
- Ding X, Lundstrom C, Huang F, Li J, Zhang ZM, Sun XM, Liang JL, Sun WD (2009) Natural and experimental constraints on formation of the continental crust based on niobium-tantalum fractionation. *Int Geol Rev* 51:473–501
- Ding X, Hu YH, Zhang H, Li CY, Ling MX, Sun WD (2013) Major Nb/Ta fractionation recorded in garnet amphibolite facies metagabbro. *J Geol* 121:255–274
- Dürr S, Alther R, Keller J, Okrusch M, Seidel E (1978) The median Aegean crystalline belt: Stratigraphy, structure, metamorphism, magmatism. In: Closs H, Roeder D, Schmidt K (eds) Alps, appenines and hellenides. Schweizerbart, Stuttgart, pp. 455–476
- Duru M, Pehlivan Ş, Şentürk Y, Yavaş F, Kar H (2004) New results on the lithostratigraphy of the Kazdağ Massif in Northwest Turkey. *Turk J Earth Sci* 13:177–186
- Eggs S, Kinsley L, Shelley J (1998) Deposition and element fractionation processes during atmospheric pressure laser sampling for analysis by ICP-MS. *Appl Surf Sci* 127:278–286
- Ellis DJ, Green DH (1979) An experimental study of the effect of Ca upon garnet-clinopyroxene Fe-Mg exchange equilibria. *Contrib Mineral Petrol* 71:12–22
- Erdoğan B, Akay E, Hasözbeğ A, Satır M, Siebel W (2013) Stratigraphy and tectonic evolution of the Kazdağ Masifi (NW Anatolia) based on field studies and radiometric ages. *Int Geol Rev* 55:2060–2082
- Ewing TA, Herman J, Rubatto D (2013) The robustness of the Zr-in-rutile and Ti-in-zircon thermometers during high-temperature



- metamorphism (Ivrea-Verbano zone, Northern Italy). *Contrib Mineral Petrol* 165:757–779
- Ferry JM, Spear FS (1978) Experimental calibration of the partitioning of Fe and Mg between biotite and garnet. *Contrib Mineral Petrol* 66: 113–117
- Ferry JM, Watson EB (2007) New thermodynamic models and revised calibrations for the Ti-in-zircon and Zr-in-rutile thermometers. *Contrib Mineral Petrol* 154:429–437
- Foley SF, Barth MG, Jenner GA (2000) Rutile/melt partition coefficients for trace elements and assessment of the influence of rutile on the trace element characteristics of subduction zone magmas. *Geochim Cosmochim Acta* 64:933–938
- Foley S, Tiepolo M, Vannucci R (2002) Growth of early continental crust controlled by melting of amphibolite in subduction zones. *Nature* 417:837–840
- Frey FA, Green DH, Roy SD (1978) Integrated Models of Basalt Petrogenesis - Study of Quartz Tholeiites to Olivine Melilitites from South Eastern Australia Utilizing Geochemical and Experimental Petrological Data. *J Petrol* 19:463–513
- Gao XY, Zheng FY, Xia XP, Chen YP (2014) U-Pb ages and trace element of metamorphic rutile from ultrahigh-pressure quartzite in the Sulu orogen. *Geochim Cosmochim Acta* 143:87–114
- Graham J, Morris RC (1973) Tungsten- and antimony substituted rutile. *Mineral Mag* 39:470–473
- Green TH (1995) Significance of Nb/Ta as an indicator of geochemical processes in the crust–mantle system. *Chem Geol* 120:347–359
- Hermann J, Spandler C, Hack A, Korsakov A (2006) Aqueous fluids and hydrous melts in high-pressure and ultra-high pressure rocks: implications for element transfer in subduction zones. *Lithos* 92:399–417
- Hodges KV, Spear FS (1982) Geothermometry, geobarometry and the Al<sub>2</sub>SiO<sub>5</sub> triple point at Mt. Moosilauke, New Hampshire. *Am Mineral* 67:118–34
- Holland TJB, Powell R (1990) An enlarged and updated internally consistent thermodynamic data set with uncertainties and correlations: the system K<sub>2</sub>O – Na<sub>2</sub>O – CaO – MgO – MnO – FeO – Fe<sub>2</sub>O<sub>3</sub> – Al<sub>2</sub>O<sub>3</sub> – TiO<sub>2</sub> – SiO<sub>2</sub> – C – H<sub>2</sub>O – O<sub>2</sub>. *J Metamorph Geol* 8:89–124
- Hornig WS, Hess PC (2000) Partition coefficients of Nb and Ta between rutile and anhydrous haplogranite melts. *Contrib Mineral Petrol* 138: 176–185
- Huang J, Xiao YL, Gao YJ, Hou ZH, Wu W (2012) Nb–Ta fractionation induced by fluid-rock interaction in subduction-zones: constraints from UHP eclogite- and vein-hosted rutile from the Dabie orogen, Central-Eastern China. *J Metamorph Geol* 30:821–842
- Jochum KP, Nehring F (2006) NIST 610: GeoReM preferred values (11/2006). *GeoReM* <http://georem.mpch-mainz.gwdg.de>
- John T, Scherer EE, Haase K, Schenk V (2004) Trace element fractionation during fluid-induced eclogitization in a subducting slab: trace element and Lu–Hf–Sm–Nd isotope systematics. *Earth Planet Sci Lett* 227:441–456
- John T, Klemm R, Klemme S, Pfänder J, Hoffmann J, Gao J (2011) Nb–Ta fractionation by partial melting at the titanite–rutile transition. *Contrib Mineral Petrol* 161:35–45
- Klemme S, Prowatke S, Hametner K, Gunther D (2005) Partitioning of trace elements between rutile and silicate melts: implications for subduction zones. *Geochim Cosmochim Acta* 69:2361–2371
- Kohn MJ, Spear FS (1990) Two new geobarometers for garnet amphibolites with applications to Southeastern Vermont. *Am Mineral* 75:89–96
- Luvizotto GL, Zack T (2009) Nb and Zr behavior in rutile during high-grade metamorphism and retrogression: An example from the Ivrea–Verbano Zone. *Chem Geol* 261:303–317
- Luvizotto GL, Zack T, Meyer HP, Ludwig S, Triebold S, Kronz A, Munker C, Stockli DF, Prowatke S, Klemme S, Jacob DE, Eynatten H (2009) Rutile crystals as potential trace element and isotope mineral standards for microanalysis. *Chem Geol* 261:346–369
- Meinhold G (2010) Rutile and its applications in earth sciences. *Earth Sci* 102:1–28
- Meinhold G, Kostopoulos D, Frei D, Himmerkus F, Reischmann T (2010) U-Pb LA-SF-ICP-MS zircon geochronology of the Serbo-Macedonian Massif, Greece: Palaeotectonic constraints for Gondwana-derived terranes in the Eastern Mediterranean. *Int J Earth Sci* 99:813–832
- Meyer M, John T, Brandt S, Klemm R (2011) Trace element composition of rutile and the application of Zr-in-rutile thermometry to UHT metamorphism (Epupa complex, NW Namibia). *Lithos* 126:388–401
- Miller C, Zanetti A, Thoni M (2007) Eclogitisation of gabbroic rocks: redistribution of trace elements and Zr in rutile thermometry in an Eo-Alpine subduction zone (Eastern Alps). *Chem Geol* 239:96–123
- Moix P, Beccaletto L, Kozur H, Hochard C, Rosselet F, Stampfli GM (2008) A new classification of the Turkish terranes and sutures and its implication for the paleotectonic history of the region. *Tectonophysics* 451:7–39
- MTA (2012) General and economic geology of the Biga Peninsula. *Spec Publ Ser* 28:326(in Turkish)
- Münker C, Pfänder JA, Weyer S, Büchl A, Kleine T, Mezger K (2003) Evolution of planetary cores and the earth–moon system from Nb/Ta systematic. *Science* 301:84–87
- Okay AI (1984) Distribution and characteristics of the Northwest Turkish blueschists. In: Robertson AHF, Dixon JE (eds) *The geological evolution of the Eastern Mediterranean*. *Geol Soc Spec Publ* 17: 455–466
- Okay AI (1986) High-pressure/low-temperature metamorphic rocks of Turkey: *Geol Soc Am Mem* 164: 333–347
- Okay AI, Tüysüz O (1999) Tethyan sutures of Northern Turkey. In: Durand B, Jolivet L, Horváth F, Séranne M (eds) *The Mediterranean basins: tertiary extension within the alpine orogen*, *Geol Soc Spec Publ*, vol 156, pp. 475–515
- Okay AI, Satır M (2000) Coeval plutonism ve metamorphism in a latest Oligocene metamorphic core complex in Northwest Turkey. *Geol Mag* 137:495–516
- Okay AI, Göncüoğlu MC (2004) The Karakaya complex: A review of data and concepts. *Turk J Earth Sci* 13:77–95
- Okay AI, Siyako M, Bürkan, KA (1991) Geology and tectonic evolution of the Biga Peninsula. In: Dewey JF (eds) *Special issue on tectonics*. *Bull Tech Uni Ist* 44: 191–255
- Okay AI, Satır M, Siebel W (2006) Pre-alpide and Mesozoic orogenic events in the Eastern Mediterranean region. *Geol Soc Spec Publ* 32: 389–405
- Okay AI, Satır M, Maluski H, Siyako M, Monie P, Metzger R, Akyüz S (1996) Paleo-and Neotethyan events in Northwest Turkey. In: Yin A, Harrison M (eds) *Tectonics of Asia*. Cambridge University Press, Cambridge, pp. 420–441
- Pickett EA, Robertson AHF, Dixon JE (1996) The Karakaya complex, NW Turkey: A palaeo tethyan accretionary complex, geology of the Black Sea region. *Geol Soc Spec Publ* 153:995–1009
- Rudnick RL, Barth M, Horn I, McDonough WF (2000) Rutile-bearing refractory eclogites: missing link between continents and depleted mantle. *Science* 287:278–281
- Scambelluri M, Bottazzi P, Trommsdorf V, Vannucci R, Hermann J, Gomez-Pugnaire MT, Lopez-Sanchez-Vizcaino V (2001) Incompatible element-rich fluids released by antigorite breakdown in deeply subducted mantle. *Earth Planet Sci Lett* 192:457–470
- Schmidt MW, Dardon A, Chazot G, Vannucci R (2004) The dependence of Nb and Ta rutile–melt partitioning on melt composition and Nb/Ta fractionation during subduction processes. *Earth Planet Sci Lett* 226:415–432
- Schmidt A, Weyer S, Mezger K, Scherer EE, Xiao YL, Hoefs J, Brey GP (2008) Rapid eclogitisation of the Dabie-Sulu UHP terrane: constraints from Lu–Hf garnet geochronology. *Earth Planet Sci Lett* 273:203–213

- Schmidt A, Weyer S, John T, Brey GP (2009) HFSE systematics of rutile-bearing eclogites: new insights into subduction zone processes and implications for the earth's HFSE budget. *Geochim Cosmochim Acta* 73:455–468
- Schuiling RD (1959) Über eine präherzynische Faltungsphase im Kazdağ Kristallin. *Bull Min Res Exp* 53:89–93
- Spear FS, Wark DA, Cheney JT (2006) Zr-in-rutile thermometry in blueschists from Sifnos, Greece. *Contrib Mineral Petrol* 152:375–385
- Stalder R, Foley SF, Brey GP, Horn I (1998) Mineral-aqueous fluid partitioning of trace elements at 900–1200 C and 3.0–5.7 GPa: new experimental data for garnet, clinopyroxene, and rutile, and implications for mantle metasomatism. *Geochim Cosmochim Acta* 62:1781–1801
- Stepanov AS, Hermann J (2013) Fractionation of Nb and Ta by biotite and phengite: implications for the “missing Nb paradox”. *Geology* 41:303–306
- Şengör AMC, Yılmaz Y (1981) Tethyan evolution of Turkey: a plate tectonic approach. *Tectonophysics* 75:181–241
- Şengün F, Yigitbas E, Tunç İO (2011) Geology and tectonic emplacement of eclogite and blueschist, Biga Peninsula, Northwest Turkey. *Turk J Earth Sci* 20:273–285
- Tatsumi Y, Nakamura N (1986) Composition of aqueous fluid from serpentinite in the subducted lithosphere. *Geochem J* 20:191–196
- Tomkins HS, Powell R, Ellis DJ (2007) The pressure dependence of the zirconium-in-rutile thermometer. *J Metamorph Geol* 25:703–713
- Watson EB, Wark DA, Thomas JB (2006) Crystallization thermometers for zircon and rutile. *Contrib Mineral Petrol* 151:413–433
- Weyer S, Muenker C, Mezger K (2003) Nb/Ta, Zr/Hf and REE in the depleted mantle: implications for the differentiation history of the crust–mantle system. *Earth Planet Sci Lett* 205:309–324
- Xia QX, Zheng YF, Hu ZC (2010) Trace elements in zircon and coexisting minerals from low-T/UHP metagranite in the Dabie orogen: implications for action of supercritical fluid during continental subduction-zone metamorphism. *Lithos* 114:385–412
- Xiao YL, Sun WD, Hoefs J, Simon K, Zhang ZM, Li SG, Hofmann AW (2006) Making continental crust through slab melting: constraints from niobium–tantalum fractionation in UHP metamorphic rutile. *Geochim Cosmochim Acta* 70:4770–4782
- Xiong XL, Adam J, Green TH (2005) Rutile stability and rutile/melt HFSE partitioning during partial melting of hydrous basalt: implications for TTG genesis. *Chem Geol* 218:339–359
- Van Achtebergh E, Ryan CG, Griffin WL (2000) GLITTER (Version 3.0, On-line interactive data reduction for LA-ICPMS). Maquarie Research Ltd
- Yiğitbaş E, Şengün F, Tunç İO (2014) Pre-Neogene tectonic units in the Biga Peninsula and an approach to geodynamic evolution of region. TUBITAK project (110Y281)
- Zack T, Luvizotto GL (2006) Application of rutile thermometry to eclogites. *Miner Petrol* 88:69–85
- Zack T, Kronz A, Foley SF, Rivers T (2002) Trace element abundances in rutiles from eclogites and associated garnet mica schists. *Chem Geol* 184:97–122
- Zack T, Moraes R, Kronz A (2004) Temperature dependence of Zr in rutile: empirical calibration of a rutile thermometer. *Contrib Mineral Petrol* 148:471–488
- Zhang JX, Yu S, Meng FC, Li JP (2009) Paired high-pressure granulite and eclogite in collision orogens and their geodynamic implications. *Acta Petrol Sin* 25:2050–2066 (in Chinese with English abstract)
- Zheng YF, Xia QX, Chen RX, Gao XY (2011) Partial melting, fluid supercriticality and element mobility in ultrahigh-pressure metamorphic rocks during continental collision. *Earth Sci* 107:342–374